Pressure-less liquid-phase sintering of aluminum-based materials

Ana Teresa Sucgang, Laurent Cuzacq, Jean-Louis Bobet, Yongfeng Lu, Jean-François Silvain

Journal of Manufacturing and Materials Processing

MDPI

Article

Pressure-Less Liquid-Phase Sintering of Aluminum-Based Materials

Ana Teresa Sucgang [1], Laurent Cuzacq [1], Jean-Louis Bobet [1], Yongfeng Lu [2] and Jean-François Silvain [1,2,*]

[1] Department of Chemistry, University of Bordeaux, CNRS, Bordeaux INP, ICMCB, UMR 5026, 33600 Pessac, France; ana-teresa.sucgang@etu.u-bordeaux.fr (A.T.S.); laurent.cuzacq97@gmail.com (L.C.); jean-louis.bobet@icmcb.cnrs.fr (J.-L.B.)

[2] Department of Electrical and Computer Engineering, University of Nebraska-Lincoln, Lincoln, NE 68588-0511, USA; yflu.email@gmail.com

* Correspondence: jean-francois.silvain@icmcb.cnrs.fr; Tel.: +33-(0)540008437

Abstract: Rapid technological advancements and the growing focus on sustainable practices have significantly expanded the potential applications of aluminum (Al) and its alloys, leading to a steady increase in demand over the years. This study investigated the densification of Al and Al-based materials using pressure-less liquid-phase sintering. Samples with 4–20 vol.% $AlSi_{12}$ sintered at 640 °C for 1 h achieved the highest relative density (RD) and the lowest global porosity (GP) without exhibiting any shape deformation. In general, increasing the amount of sintering aid improves the density of the samples. This was confirmed by microstructural analysis using SEM, which revealed the progression of density—from initial particle coalescence at 4 vol.% $AlSi_{12}$ to the development of microstructures with filled pores and well-defined grain boundaries at 20 vol.% $AlSi_{12}$. X-ray diffraction (XRD) analysis also revealed an expanded lattice parameter, with minimal microstrain and a crystallite size closely resembling those of the initial Al powder. Samples with a relative density greater than 90% demonstrated thermal conductivities ranging from 170 to 200 W/mK and an average hardness of 29 HV5. Densification was further enhanced by increasing the compaction pressure from 50 MPa to 100–200 MPa for samples containing 12–20 vol.% $AlSi_{12}$. The Al-based material compacted at 200 MPa and with 15 vol.% $AlSi_{12}$ achieved the highest RD of approximately 99%. It exhibited a thermal conductivity of 195 W/mK at 30 °C and 190 W/mK at 70 °C, along with a hardness of 30 HV5.

Keywords: pressure-less liquid phase sintering (LPS); relative density (RD) and global porosity (GP); thermal conductivity and hardness; Al and Al-based materials

Academic Editors: Xuedao Shu and Song Zhang

Received: 21 November 2024
Revised: 24 December 2024
Accepted: 25 December 2024
Published: 26 December 2024

Citation: Sucgang, A.T.; Cuzacq, L.; Bobet, J.-L.; Lu, Y.; Silvain, J.-F. Pressure-Less Liquid-Phase Sintering of Aluminum-Based Materials. *J. Manuf. Mater. Process.* **2025**, *9*, 4. https://doi.org/10.3390/jmmp9010004

1. Introduction

Aluminum (Al) has been the most widely used non-ferrous metal for several years [1,2], holding an over one-third share of the total type-based non-ferrous metals market in 2022 [2]. The standout properties of Al—such as low density, excellent corrosion resistance, good machinability, and high thermal and electrical conductivity—make it essential for diverse applications across aerospace, automotive, machinery and tools manufacturing, building construction, packaging, and electronics industries [1,3]. However, similarly to any other metals, pure Al lacks the mechanical properties needed for structural integrity. This is usually addressed with the addition of other elements to improve the strength of lightweight Al alloys [1,4–6].

There are several processes to prepare Al and its alloys; one of which is via the powder metallurgy (PM) route. The PM route is a net- or near-net-shape manufacturing process that brings added advantages to the Al and Al alloys market, offering both economic and environmental benefits [1,3,7,8]. However, despite these benefits, the market and research progress for this process stagnated from the 1970s, until gaining renewed momentum in the last decade. One identified limitation is the oxidation susceptibility of Al and Al alloy powders, which hinders bonding among particles and, thus, affects the densification and, so, the properties of the alloy. High reactivity of Al with tooling materials leads to increased manufacturing costs due to degradation. Another limitation is the insufficient wear resistance and tensile strength of many Al alloys [1,3,4,7–9]. Finally, another limitation is the high pressure generally applied during the sintering. Indeed, this high pressure generally increases a lot the manufacturing costs [10].

Liquid phase sintering (LPS) is one of the approaches that have been used to solve the inevitable formation of Al oxides. This process is a type of sintering in which both liquid and solid phases coexist during part of the sintering step. The liquid phase originates one of the alloying elements through a eutectic formation. The LPS process offers several advantages: it enables a lower sintering temperature for the liquid phase of the sintering aid, enhances densification by lowering the activation energy for atomic diffusion, improves particle bonding through surface wetting, allows for controlled porosity and microstructure by adjusting composition and sintering conditions, and shortens processing times due to improved densification kinetics. [3,8,11,12].

Similarly, to conventional press-and-sinter methods, the sintering step in LPS dictates the properties of Al materials. Sintering conditions, such as temperature, dwell time, cooling rate, and alloying elements or additive composition are the common parameters being modified to achieve certain sets of desired properties. An optimized sintering temperature is crucial, as it provides enough thermal energy to overcome intermolecular forces and accelerate particle diffusion without causing coarsening or potential shape deformation [13]. Alloying elements or additive compositions, on the other hand, can significantly influence the properties of the final material and enhance the densification process [9,14]. While sintering time is a minor variable, optimizing it can positively impact material properties and yield economic benefits in the process [12,13]. Compaction and sintering pressures play crucial roles in both the densification and the microstructure development, which, in turn, affect the final properties of the material.

Despite past setbacks in the process development of the PM route of Al and its alloys, the previously mentioned benefits have led to renewed interest in these materials. This resurgence aims to overcome existing limitations and explore the potential for producing aluminum materials with properties tailored to specific applications. The aim of the work described in this paper is to densify Al and Al-based materials using a pressure-less LPS. The effects of the process on the material's microstructures and thermal and mechanical properties were investigated.

2. Methodology

2.1. Sample Preparation

Spherical Al powder with an average particle size of 7 μm (ULT0665, Néochimie, Cergy-Pontoise, France) and pre-alloyed Al-Si 12.2 atomic%, referred to as $AlSi_{12}$ powder, with a melting temperature of 577 °C and an average particle size of 18 μm (Toyo Aluminum KK, Kosan, Japan) were the raw materials used in experiments. Due to high compositional uniformity, $AlSi_{12}$ was used as the sintering aid or additive instead of a pure silicon to improve sample homogeneity, prevent possible segregation in the matrix, and increase the major phase solubility [15].

The Al and $AlSi_{12}$ powders were blended and homogenized for 5 min at 1200 rpm using a planetary mixer (Thinky ARE250CE, Tokyo, Japan). For initial consolidation of the loose powders, compaction using a cold uniaxial press was performed and verified in a pressure range of 50 to 200 MPa.

2.2. Sintering Parameters Optimization

Al-based compacts with varied compositions (4–20 vol.%) of $AlSi_{12}$ were sintered (Beijing JinYeHong Metallurgical Mechanical Equipment Corp Ltd., Beijing, China) at 620, 640, and 650 °C for 30 and 60 min in an argon atmosphere with 5 vol.% hydrogen. The overall system pressure was maintained at ≤ 0.2 bar, with the following steps. A first ramp with a rate of 5 °C/min from 20 to 410 °C and a 10 min dwell allowed the lubricant to be removed. Then, another ramp with a rate of 10 °C/min from 410 °C to the sintering temperature (between 620 and 650 °C) and a dwell time of 30 min or 1 h was used to sinter the parts. Finally, a cool rate of 10 °C/min was applied to cool down the furnace.

2.3. Characterization

Phase and composition identification was performed using X-ray diffraction (XRD) using a Philips PANalytical X'Pert Pro, Madison, WI, USA, equipped with a copper source ($\lambda_{K\alpha1}$ = 0.15405 nm and $\lambda_{K\alpha2}$ = 0.15443 nm). Measurements were taken between 2θ = 10 and 80 °, with a 0.02 ° (2θ) step and a 2.022 ° (2θ) active width in the detector. Microstructural analysis of the samples was also performed using a scanning electron microscope (SEM; Tescan, VEGA © II SBH, Brno, Czech Republic). The density of the composite materials was measured using the Archimedes method [Sartorius Analitic® balance (d = 0.1 mg)].

To determine the effect of varied $AlSi_{12}$ compositions on the mechanical and thermal properties of the material, a Vickers hardness test with a 49 N load (Wilson Vickers hardness tester –WILSON Hardness,, New York, USA, Vickers 452 SVD) and thermal diffusivity tests at 30 and 70 °C using laser pulse method (MicroFlash NETZSCH LFA 457®, Selb, Germany) were performed.

For each characterization, the measurement was made 3 times to ensure the accuracy and repeatability of the results.

3. Results and Discussion

Densification of the Al-based material via free LPS began with preliminary powder compaction at 50 MPa, followed by optimization of the sintering aid composition, temperature, and dwell time. Initial consolidation of the samples resulted in an average green RD of 75 %. As shown in Figure 1, the RD of the pellets without $AlSi_{12}$ remained unchanged after sintering. In contrast, all the samples mixed with the pre-alloyed powder exhibited higher RD, and consequently, lower GP when sintered at temperatures of 640 and 650 °C for a 1 h dwell time. Although $AlSi_{12}$ was expected to melt at its eutectic temperature of 577 °C [16,17], the pressure-less sintering environment impacted the particle diffusion, necessitating higher thermal energy to enhance atomic mobility. The effect of the dwell time was highlighted by the 4 % $AlSi_{12}$ pellets sintered at 640 and 650 °C. With limited amount of sintering aid, the samples were provided with sufficient diffusion time for effective pore filling and elimination.

Figure 1 indicates that as the $AlSi_{12}$ composition increased, the RD also increased, while the GP decreased. This outcome is logical, as the addition of more sintering aid promotes particle bonding, leading to improved packing and lesser pores. However, shape deformation began to appear in samples with higher $AlSi_{12}$ composition (15 and 20 vol.%) when sintered at 650 °C, for both 30 min and 1 h dwell times (cf. Figure 2 framed pellets).

The substantial large amount of the sintering aid, combined with sufficient thermal energy, may have caused $AlSi_{12}$ to leak from the samples. A better set of results was achieved with the densified pellets sintered at 640 °C for 1 h; therefore, further experiments and characterizations were conducted on these samples.

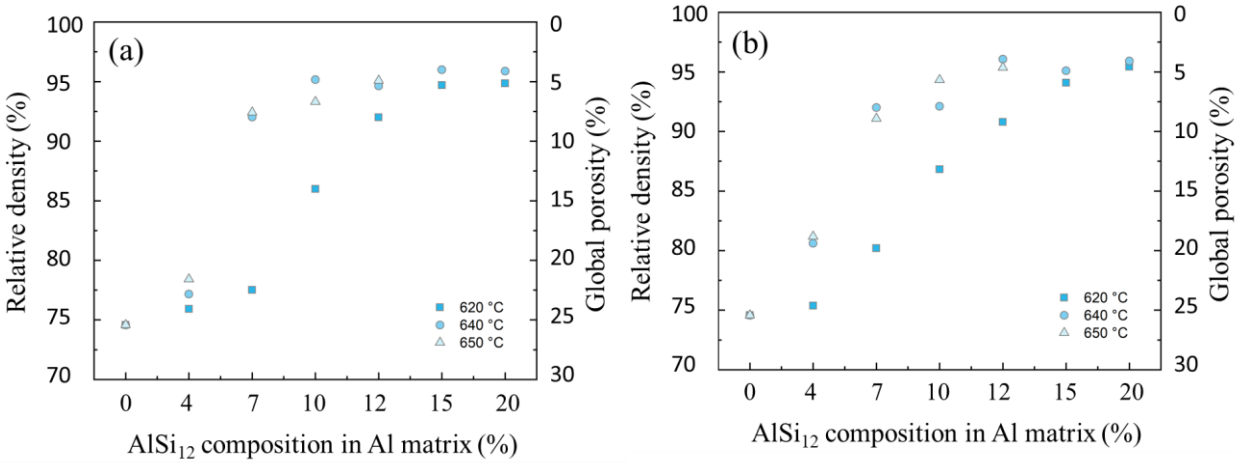

Figure 1. Effect of $AlSi_{12}$ composition on relative density and global porosity of Al and Al-based samples sintered at 640 °C for (**a**) 30 min and (**b**) 1 h in an Ar-H_2 gas mixture.

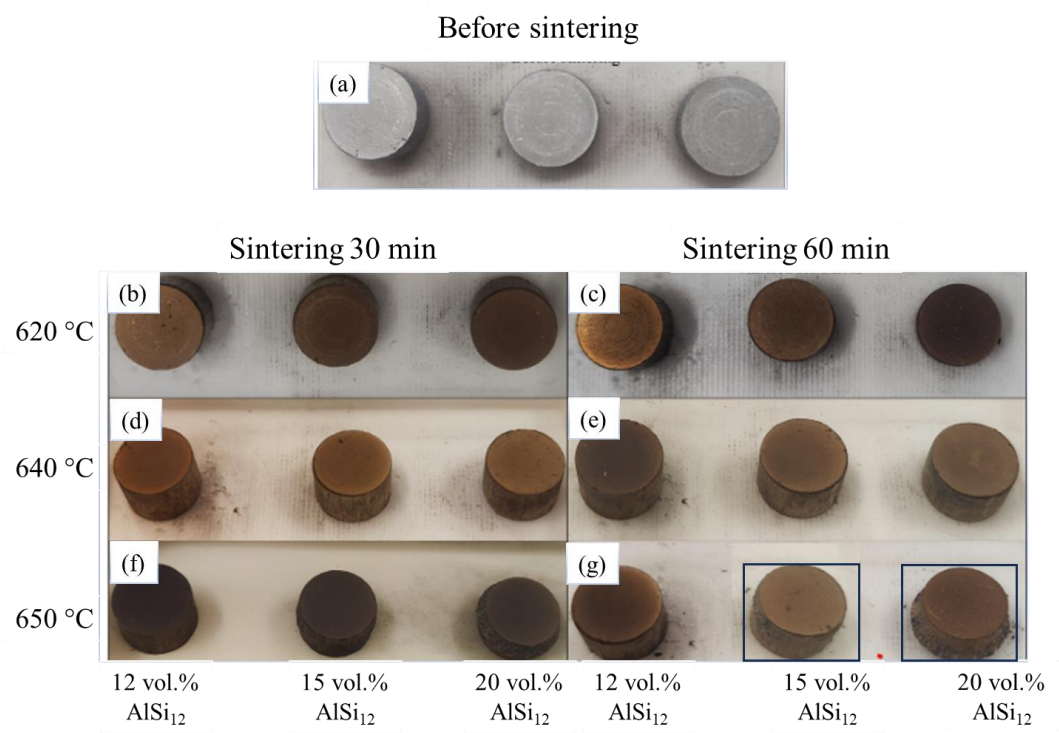

Figure 2. Pellets (diameter 6 mm) with high $AlSi_{12}$ compositions: (**a**) before and after sintering at (**b**,**c**) 620, (**d**,**e**) 640, and (**f**,**g**) 650 °C for 30 min and 1 h in an Ar-H_2 atmosphere.

The quantitative assessment of RD and GP was further supported by SEM micrographs of cryo-fractured samples (Figure 3). The evolution of the sample density was observed starting from the Al matrix with 4 vol.% $AlSi_{12}$, where sintering necks formed and initial grain growth began, up to the sample with 20 vol.% $AlSi_{12}$, which displayed a more homogeneous microstructure. Additionally, the chemically etched samples in Figure 4 revealed a gradual filling of pores and grain boundaries as the $AlSi_{12}$ composition increased. The reduction in pore number and size, along with observed grain growth, provides a

clear picture of the densification progress as influenced by the amount of sintering aid. In contrast, the sample containing only Al powder, processed under the same conditions as the other Al-based pellets, exhibited a high level of porosity.

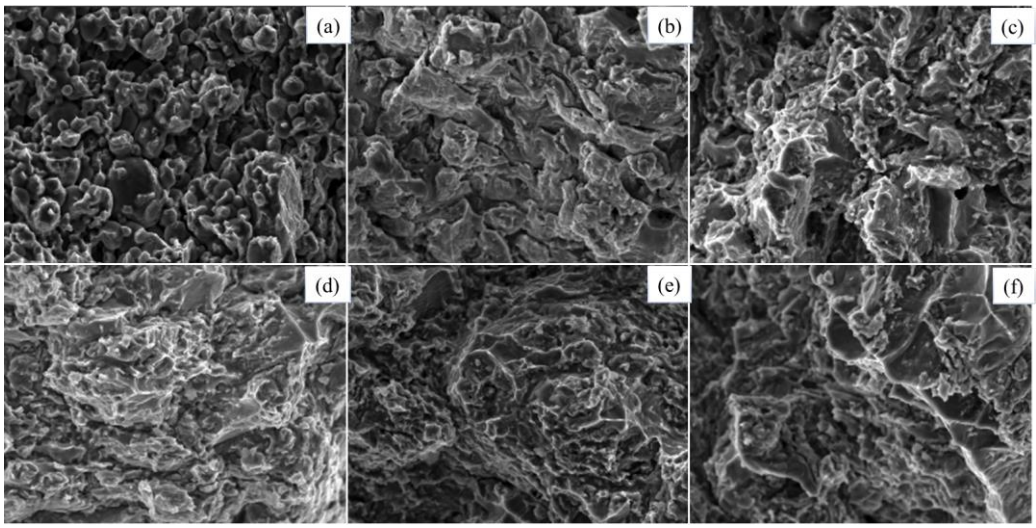

Figure 3. SEM micrographs of cryo-fractured samples with varying $AlSi_{12}$ composition: (**a**) 4 %; (**b**) 7 %; (**c**) 10 %; (**d**) 12 %; **(e)** 15 %; and (**f**) 20 %, compacted at 50 MPa and sintered at 640 °C for 1 h under Ar-H_2 gas.

Qualitative assessment using XRD analysis confirmed the presence of alumina (Al_2O_3) layers in the Al powders used (Figure 4). The peaks corresponding to the oxide phase noticeably decreased and eventually disappeared as the relative density (RD) of the samples increased. This can be attributed to the LPS process, which improves the wetting of the Al_2O_3 layer, increasing its dissolution in the liquid. The XRD data also confirmed an increasing amount of Si in each sample, evidenced by the rising intensity of the peaks corresponding to silicon. The overall peak pattern aligned with the previously reported data from several studies [18–24].

The evolution of cell parameters in all samples was also determined using the Le Bail pattern decomposition method. If an alloy forms during the process, substitutional alloying is likely, given the relative similar atomic radii of Al (1.43 Å) and Si (1.32 Å). However, the unit cell parameter expanded for all samples, approaching the reference value of Al as measured by XRD (4.0495 Å) as the RD increased.

Additional information was obtained from the microstrain and crystallite size measurements using the Williamson and Hall method. Regardless of the initial pressure conditions (50 and 100 MPa), Al-based samples had an average crystallite size of 51 nm (46–58 nm) and a microstrain of 0.021 % (0.012–0.040 %). These are close to the crystallite size (50 nm) and microstrain (0.033 %) of the pure Al powder used. This is consistent with the absence of broadening of peaks observed relative to the peaks of the starting Al powder.

Moreover, the narrow range of unit cell parameter values indicates consistent sintering conditions, which led to improved packing without inducing extensive grain growth [25–27]. The lack of a clear trend among samples may be attributed to the absence of external pressure in the LPS process used. Densification mainly depended on the liquid phase and atomic diffusion, which were influenced by particle arrangement and the presence of pores. Based on the microstructural analyses performed, the sintered pellets showed enhanced particle bonding and pore filling rather than alloy formation.

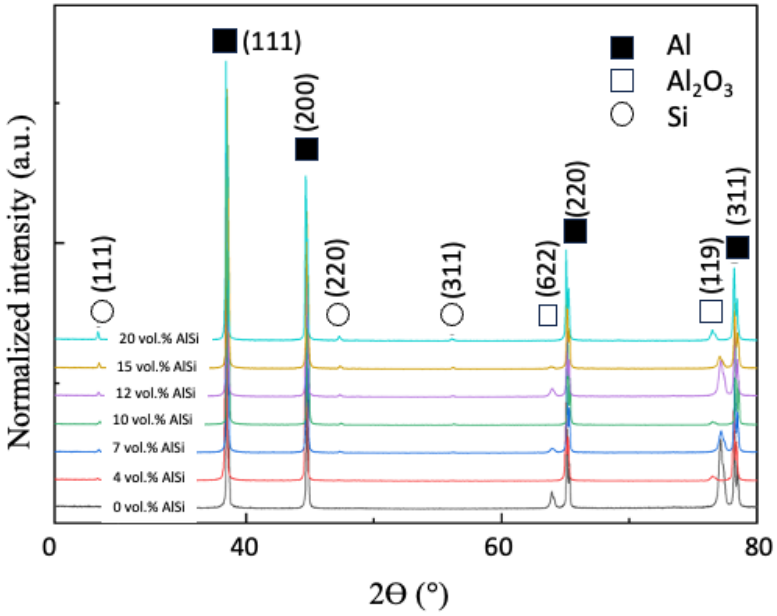

Figure 4. XRD analysis of densified Al-based pellets with varying $AlSi_{12}$ compositions (4–20 vol.%), sintered at 640 °C for 1 h under Ar-H_2 atmosphere.

The thermal conductivity (TC) of pure Al, as reported by Ho et al. (1972), is 237 W/mK at 30 °C and 240 W/mK at 70 °C, while for pure Si it is 148 W/mK at 30 °C and 119 W/m K at 70 °C [28]. Excellent thermal conductivity of Al, combined with its lightweight, makes it ideal for applications such as heat dissipation in electronics. However, the addition of a sintering aid, along with its amount and distribution within the matrix, negatively affects the TC [29,30]. The Si content mixed in all samples was limited to low concentrations (0.5–2.4 atomic% Si, which correspond to 4 to 20 vol.% of $AlSi_{12}$) to prevent significant loss of the thermal properties in the Al material. This was observed from the samples containing 4–20 vol.% $AlSi_{12}$ with TCs measured to be 170–200 W/mK at 30 and 70 °C (Figure 5). The sample with no sintering aid, on the other hand, exhibited a very low conductivity of about 15 W/mK at 30 and 70 °C, which is attributed to the low densification. The significant improvement in TC by adding $AlSi_{12}$ is mainly due to the density increase and pore reduction, which enhanced the interparticle bonding to facilitate a more efficient heat transfer. Additionally, since a solid solution of Si likely did not form, the negative effect of the additive on TC was reduced, as there was no interference with electron thermal conduction within the Al matrix [29]. While the obtained TC values were lower than those of pure aluminum, they were still higher than other reported measurements for Al-Si alloys [14,30–32].

The addition of $AlSi_{12}$ in the Al-based samples had an overall positive effect on hardness, attributed to the improved material density compared to samples without a sintering aid. This was evident with the results shown in Figure 5, which demonstrate that as the density of samples increased, hardness also increased. However, these hardness values were lower than those reported for other Al-Si alloys (> 40 HV) [33–37] and were closer to the hardness of commercially available pure Al (~ 30 HV5) [34]. This is because the Al-based materials fabricated in this study were only densified rather than alloyed. Alloying is a common technique employed to strengthen metals by impeding dislocation movements. Its effectiveness is influenced by several factors, such as the alloying process, amount of alloying element, and the manner in which it dissolves within the matrix [34,35].

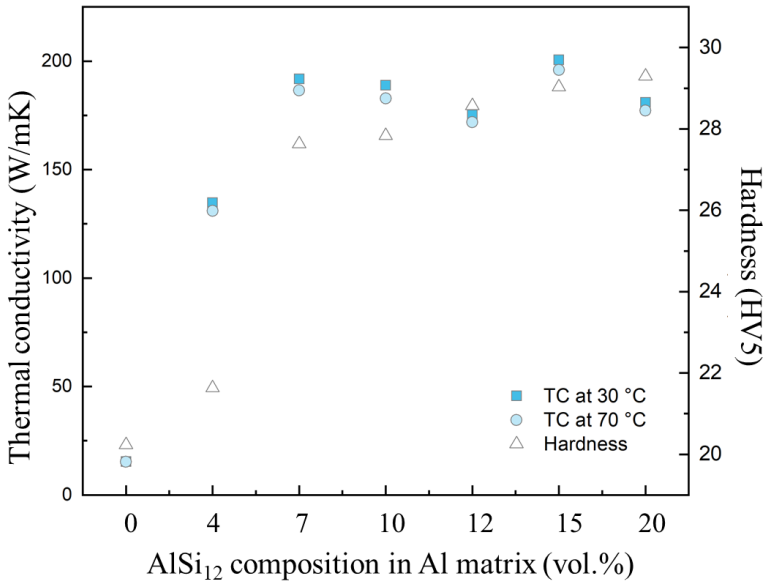

Figure 5. Hardness and thermal conductivity of pellets sintered at 640 °C for 1 h.

Processing of the Al and Al-based materials was further improved by increasing the compaction pressure from 50 MPa to 100, 150, and 200 MPa on samples containing 12 to 20 vol.% $AlSi_{12}$. Similar sintering conditions and characterizations were employed on the densified pellets. The green RDs obtained for samples compacted at 100, 150, and 200 MPa were 80, 85, and 87 %, respectively. As shown in Figure 6, no change in RDs was observed from Al samples without the sintering aid, while 95–98.6 % RDs and GPs smaller than 5 % were obtained from samples containing 12–20 vol.% $AlSi_{12}$. Cracks formed at the bottom of the pellet compacted at 200 MPa and containing 20 vol.% $AlSi_{12}$. This is likely due to the excessive compaction pressure and the amount of additive used, which introduced stresses into the material.

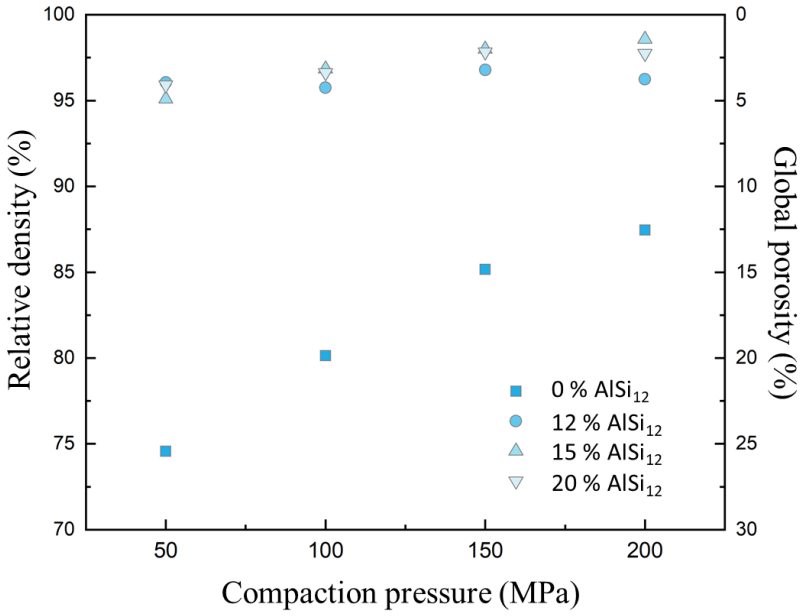

Figure 6. Effect of compaction pressure on relative density and global porosity of Al and Al-based samples sintered at 640 °C for 1 h under Ar-H_2 atmosphere.

SEM analysis revealed tightly packed structures with fewer and smaller pores in samples compacted at higher pressures. Additionally, the XRD results for samples

compacted at higher pressures were similar to those compacted at 50 MPa, with the exception of some small peak broadening observed in the (111) and (200) planes for samples compacted at 100 MPa with 1, 5, and 20 vol.% $AlSi_{12}$, and at 150 MPa with 20 vol.% $AlSi_{12}$. However, all other parameters, such as the lattice parameter, crystallite size, and microstrain, showed similar behavior to their equivalent samples compacted at 50 MPa. Moreover, the thermal property and hardness of these materials did not significantly change as well. It can be observed from Figure 7a that the thermal conductivity at 30 °C (180–200 W/mK) was of the same range as what was observed for samples compacted at 50 MPa. Meanwhile, the average hardness for the Al-based materials containing 12–20 vol.% $AlSi_{12}$ that were compacted at higher pressures (100–200 MPa) was 30 HV5. This value is very close to the average hardness (29 HV5) of the densified samples with the same $AlSi_{12}$ composition but compacted only at 50 MPa (Figure 7b).

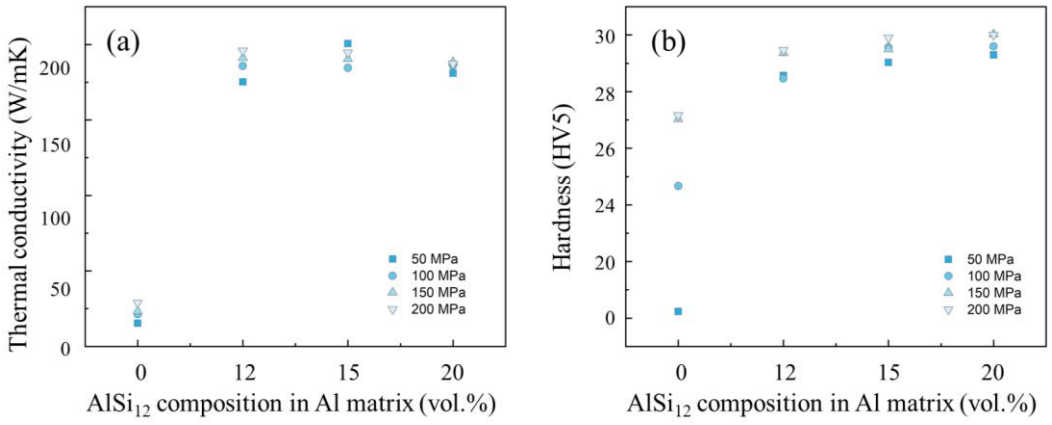

Figure 7. Thermal conductivity at (**a**) 30 °C and (**b**) hardness of densified Al and Al-based pellets compacted at higher pressures and with varying $AlSi_{12}$ compositions.

4. Conclusions

This study successfully densified Al and Al-based materials using the pressure-less LPS process, with $AlSi_{12}$ serving as the sintering aid. The samples densified and compacted at 50 MPa and containing 4–20 vol.% $AlSi_{12}$ at 640 °C for 1 h exhibited RD of 81–96% and GP of 4–20%. SEM characterization revealed that the process induced grain boundaries and pore filling, effectively consolidating the Al and Al-based materials. Additionally, comparison of XRD results between samples and raw materials showed no broadening of the Al peaks for all the sintered pellets. All samples exhibited expanded cell parameters, with average crystallite size and microstrain values similar to those of the initial Al powder. Effects of the densification process on the thermal and mechanical properties of the materials were also evaluated. Samples with a relative density (RD) greater than 90% exhibited thermal conductivity in the range of 170–200 W/mK, a competitive value comparable to that of Al-Si alloys. The average hardness of these materials was 29 HV5, close to that of a commercially available Al (30 HV5). The density was further improved by increasing the compaction pressure from 50 to 100–200 MPa, achieving a maximum RD of about 99 %, a thermal conductivity about 190 W/m K, and a hardness of 30 HV5.

Author Contributions: This work was completed through the contributions of all authors. The individual contributions were supervision and conceptualization: J.-F.S.; manuscript writing: A.T.S., L.C., J.-F.S., and Y.L.; material elaboration, characterization, and post-treatment: A.T.S., L.C.; XRD analysis: J.-L.B. All authors have read and agreed to the published version of the manuscript.

Funding: This research received no external funding.

Data Availability Statement: All the data required to evaluate the conclusions presented in this paper are included within this paper. The datasets generated during the current study are available from the corresponding author upon reasonable request.

Acknowledgments: The Institute of Condensed Matter Chemistry of Bordeaux (ICMCB) is acknowledged for their provision of equipment and financial support.

Conflicts of Interest: The remaining authors declare that the research was conducted in the absence of any commercial or financial relationships that could be construed as a potential conflict of interest.

References

1. Totten, G.E.; MacKenzie, D.S. (Eds.) *Handbook of Aluminum: Vol. 1: Physical Metallurgy and Processes*; CRC Press: Boca Raton, FL, USA, 2003. https://doi.org/10.1201/9780203912591
2. M.P. Research Cognitive Market, Non Ferrous Metals Market Size Was USD 711.02 Billion in 2022!, Cognitive Market Research. Available online: https://www.cognitivemarketresearch.com/non-ferrous-metals-market-report (accessed on 12 December 2024).
3. Qian, M.; Schaffer, G.B. Sintering of aluminium and its alloys. In *Sintering of Advanced Materials*; Elsevier: Amsterdam, The Netherlands, 2010; pp. 291–323. https://doi.org/10.1533/9781845699949.3.291.
4. Davis, J.R. *Alloying: Understanding the Basics*; ASM International: Almere, The Netherlands, 2001. https://doi.org/10.31399/asm.tb.aub.9781627082976.
5. Ahmed, M.S.; Anwar, M.S.; Islam, M.S.; Arifuzzaman, M. Experimental study on the effects of three alloying elements on the mechanical, corrosion and microstructural properties of aluminum alloys. *Results Mater.* **2023**, *20*, 100485. https://doi.org/10.1016/j.rinma.2023.100485.
6. Godbole, K.; Bhushan, B.; Narayana Murty, S.V.S.; Mondal, K. Al-Si controlled expansion alloys for electronic packaging applications. *Prog. Mater. Sci.* **2024**, *144*, 101268. https://doi.org/10.1016/j.pmatsci.2024.101268.
7. Judge, W.; Kipouros, G. Powder Metallurgy Aluminum Alloys: Structure and Porosity. In *Encyclopedia of Aluminum and Its Alloys, Two-Volume Set (Print)*; CRC Press: Boca Raton, FL, USA, 2018. ISBN 978-1-351-04563-6.
8. Schaffer, G.B.; Sercombe, T.B.; Lumley, R.N. Liquid phase sintering of aluminium alloys. *Mater. Chem. Phys.* **2001**, *67*, 85–91. https://doi.org/10.1016/S0254-0584(00)00424-7.
9. Mosher, W.G.; Kipouros, G.J.; Caley, W.F.; Donaldson, I.W.; Bishop, D.P. On development of hypoeutectic aluminium-silicon powder metallurgy alloy. *Powder Metall.* **2011**, *54*, 432–439. https://doi.org/10.1179/003258910X12785770528172.
10. Wu, L.; Yu, Z.; Liu, C.; Ma, Y.; Huang, Y.; Wang, T.; Yang, L.; Yan, H.; Liu, W. Microstructure and tensile properties of aluminum powder metallurgy alloy prepared by a novel low-pressure sintering. *J. Mater. Res. Technol.* **2021**, *14*, 1419–1429. https://doi.org/10.1016/j.jmrt.2021.07.074.
11. Arribas, I.; Martín, J.M.; Castro, F. The initial stage of liquid phase sintering for an Al–14Si–2.5Cu–0.5Mg (wt%) P/M alloy. *Mater. Sci. Eng. A* **2010**, *527*, 3949–3966. https://doi.org/10.1016/j.msea.2010.02.078.
12. German, R.M. *Liquid Phase Sintering*; Springer International Publishing: Cham, Switzerland, 2013. ISBN 978-1-4899-3599-1.
13. Su, S.S. *Development of Hypereutectic A1-Si Based P/M Alloys*; University of Birmingham: Birmingham, UK, 2012.
14. Angadi, B.M.; Hiremath, C.R.; Reddy, A.C.; Katti, V.V.; Kori, S.A. Studies on the thermal properties of hypereutectic Al–Si alloys by using transient method. *J. Mech. Eng.* **2014**, *2*, 536–544.
15. Cuzacq, L.; Atchi, I.; Bobet, J.-L.; Lu, Y.; Silvain, J.-F. Pressureless sintering of Al/diamond materials using AlSi12 liquid phase. *Mater. Lett.* **2025**, *381*, 137788. https://doi.org/10.1016/j.matlet.2024.137788.
16. Vora, P.; Mumtaz, K.; Todd, I.; Hopkinson, N. AlSi12 in-situ alloy formation and residual stress reduction using anchorless selective laser melting. *Addit. Manuf.* **2015**, *7*, 12–19. https://doi.org/10.1016/j.addma.2015.06.003.
17. Li, W.-Y.; Zhang, C.; Guo, X.P.; Zhang, G.; Liao, H.L.; Coddet, C. Deposition characteristics of Al–12Si alloy coating fabricated by cold spraying with relatively large powder particles. *Appl. Surf. Sci.* **2007**, *253*, 7124–7130. https://doi.org/10.1016/j.apsusc.2007.02.142.
18. Vanzetti, M.; Pavel, M.J.; Williamson, C.J.; Padovano, E.; Pérez-Andrade, L.I.; Weaver, M.; Brewer, L.N.; Bondioli, F.; Fino, P. Design and Characterization of Innovative Gas-Atomized Al-Si-Cu-Mg Alloys for Additive Manufacturing. *Metals* **2023**, *13*, 1845. https://doi.org/10.3390/met13111845.
19. Mohammed, S.H.; Noori, F.T.M. Effect of Cooling Rates and rapidly quenched on Al-Si alloy. *Al-Mustansiriyah J. Sci.* **2022**, *33*, 77–81. https://doi.org/10.23851/mjs.v33i1.1084.

20. Guo, J.; Wang, F.; Zhang, S.; Zhou, Y.; Zhu, L. Effect of High-Frequency Electric Pulse on the Solidification Microstructure and Properties of Hypoeutectic Al-Si Alloy. *Materials* **2024**, *17*, 468. https://doi.org/10.3390/ma17020468.
21. Mohammed, M.M.M.; Elkady, O.A.; Abdelhameed, A.W. Effect of Alumina Particles Addition on Physico-Mechanical Properties of AL-Matrix Composites. *Open J. Met.* **2013**, *3*, 72–79. https://doi.org/10.4236/ojmetal.2013.34011.
22. Kumar, S.; Mote, V.D.; Prakash, R.; Kumar, V. X-ray Analysis of α-Al_2O_3 Particles by Williamson–Hall Methods. *Mater. Focus* **2016**, *5*, 545–549. https://doi.org/10.1166/mat.2016.1345.
23. Jang, S.; Gun Oh, D.; Kim, H.; Hyun Kim, K.; Khivantsev, K.; Kovarik, L.; Hun Kwak, J. Controlling the Phase Transformation of Alumina for Enhanced Stability and Catalytic Properties. *Angew. Chem. Int. Ed.* **2024**, *63*, e202400270. https://doi.org/10.1002/anie.202400270.
24. Lee, J.S.; Kim, H.S.; Park, N.-K.; Lee, T.J.; Kang, M. Low temperature synthesis of α-alumina from aluminum hydroxide hydrothermally synthesized using $[Al(C_2O_4)x(OH)y]$ complexes. *Chem. Eng. J.* **2013**, *230*, 351–360. https://doi.org/10.1016/j.cej.2013.06.099.
25. Ungar, T. Microstructural parameters from X-ray diffraction peak broadening. *Scr. Mater.* **2004**, *51*, 777–781. https://doi.org/10.1016/j.scriptamat.2004.05.007.
26. Bruno, G.; Efremov, A.M.; Levandovskyi, A.N.; Clausen, B. Connecting the macro- and microstrain responses in technical porous ceramics: Modeling and experimental validations. *J. Mater. Sci.* **2011**, *46*, 161–173. https://doi.org/10.1007/s10853-010-4899-0.
27. Soares, E.; Bouchonneau, N.; Alves, E.; Alves, K.; Araújo Filho, O.; Mesguich, D.; Chevallier, G.; Laurent, C.; Estournès, C. Microstructure and Mechanical Properties of AA7075 Aluminum Alloy Fabricated by Spark Plasma Sintering (SPS). *Materials* **2021**, *14*, 430. https://doi.org/10.3390/ma14020430.
28. Ho, C.Y.; Powell, R.W.; Liley, P.E. Thermal Conductivity of the Elements. *J. Phys. Chem. Ref. Data* **1972**, *1*, 279–421. https://doi.org/10.1063/1.3253100.
29. Mujahid, M.; Engel, N.N.; Chia, E.H. Effect of alloying elements on the conductivity of aluminum alloys. *Scr. Metall.* **1979**, *13*, 887–893. https://doi.org/10.1016/0036-9748(79)90181-9.
30. Zhang, A.; Li, Y. Thermal Conductivity of Aluminum Alloys—A Review. *Materials* **2023**, *16*, 2972. https://doi.org/10.3390/ma16082972.
31. Razin, A.A.; Ahammed, D.S.-S.; Khan, A.A.; Kaiser, M.S. THERMOPHYSICAL PROPERTIES OF HYPOEUTECTIC, EUTECTIC AND HYPEREUTECTIC Al-Si AUTOMOTIVE ALLOYS UNDER AGEING TREATMENT. *J. Chem. Technol. Metall.* **2024**, *59*, 673–682. https://doi.org/10.59957/jctm.v59.i3.2024.22.
32. Kong, Z.; Huang, H.; Li, Y.; Yu, B.; Chen, B.; Li, R. Effect of sintering process on microstructure and properties of Al–Si alloy made by powder metallurgy for electronic packaging application. *Mater. Res. Express* **2023**, *10*, 66506–. https://doi.org/10.1088/2053-1591/acd990.
33. Pichumani, S.; Srinivasan, R.; Venkatraman Ramamoorthi, S. Investigation on mechanical behavior and material characteristics of various weight composition of SiCp reinforced aluminium metal matrix composite. In Proceedings of the International Conference on Advances in Materials and Manufacturing Applications (IConAMMA-2017), Bengaluru, India, 2017. https://doi.org/10.1088/1757-899X/310/1/012082.
34. Tirth, V.; Arabi, A. Effect of liquid forging pressure on solubility and freezing coefficients of cast aluminum 2124, 2218 and 6063 alloys. *Arch. Metall. Mater.* **2020**, *65*, 357–366. https://doi.org/10.24425/amm.2020.131738.
35. Hatti, G.; Vishwanath, V.H.; Dinesh, K.R. Effect of Silicon Content on wear and Hardness of Al-Si Alloys. *IOP Conf. Ser. Mater. Sci. Eng.* **2021**, *1065*, 12010. https://doi.org/10.1088/1757-899X/1065/1/012010.
36. Jayasheel Kumar, J.K.K.; Ramesha, C.M. Evaluation of Vickers Hardness Number of Al-Si Alloy Under Heat Treated Conditions. *Int. J. Eng. Adv. Technol.* **2021**, *10*, 222–227. https://doi.org/10.35940/ijeat.F3006.0810621.
37. Saravanan, R.; Sellamuthu, R. *Determination of the Effect of Si Content on Microstructure, Hardness and Wear Rate of Surface-refined Al-Si Alloys*; Elsevier Ltd.: Amsterdam, The Netherlands, 2014; pp. 1348–1354. https://doi.org/10.1016/j.proeng.2014.12.415.